OPEN ACCESS Freely available online

PLoS GENETICS

Cancer-Associated Splicing Variant of Tumor Suppressor AIMP2/p38: Pathological Implication in Tumorigenesis

Jin Woo Choi[1], Dae Gyu Kim[1], Al-Eum Lee[1], Hye Rim Kim[1], Jin Young Lee[1], Nam Hoon Kwon[1], Young Kee Shin[2], Soon-Kyung Hwang[3], Seung-Hee Chang[3], Myung-Haing Cho[3], Yoon-La Choi[4], Jhingook Kim[5], Seung Hyun Oh[6], Bora Kim[6], Soo-Youl Kim[6], Hyo-Sung Jeon[7], Jae Yong Park[8], Hyunseok Peter Kang[9], Bum Joon Park[10], Jung Min Han[1,11], Sunghoon Kim[1,11]*

1 Medicinal Bioconvergence Research Center, Seoul National University, Seoul, Korea, **2** Laboratory of Molecular Pathology, College of Pharmacy, Seoul National University, Seoul, Korea, **3** College of Veterinary Medicine, Seoul National University, Seoul, Korea, **4** Department of Pathology, Samsung Medical Center, Sungkyunkwan University School of Medicine, Seoul, Korea, **5** Department of Thoracic and Cardiovascular Surgery, Samsung Medical Center, Sungkyunkwan University School of Medicine, Seoul, Korea, **6** National Cancer Center, Research Institute, Goyang, Korea, **7** Department of Biochemistry, School of Medicine, Kyungpook National University, Daegu, Korea, **8** Department of Internal Medicine, School of Medicine, Kyungpook National University, Daegu, Korea, **9** Department of Pathology and Laboratory Medicine, Roswell Cancer Park Institute, Buffalo, New York, United States of America, **10** Department of Molecular Biology, Pusan National University, Pusan, Korea, **11** WCU Department of Molecular Medicine and Biopharmaceutical Sciences, Seoul National University, Suwon, Korea

Abstract

Although ARS-interacting multifunctional protein 2 (AIMP2, also named as MSC p38) was first found as a component for a macromolecular tRNA synthetase complex, it was recently discovered to dissociate from the complex and work as a potent tumor suppressor. Upon DNA damage, AIMP2 promotes apoptosis through the protective interaction with p53. However, it was not demonstrated whether AIMP2 was indeed pathologically linked to human cancer. In this work, we found that a splicing variant of AIMP2 lacking exon 2 (AIMP2-DX2) is highly expressed by alternative splicing in human lung cancer cells and patient's tissues. AIMP2-DX2 compromised pro-apoptotic activity of normal AIMP2 through the competitive binding to p53. The cells with higher level of AIMP2-DX2 showed higher propensity to form anchorage-independent colonies and increased resistance to cell death. Mice constitutively expressing this variant showed increased susceptibility to carcinogen-induced lung tumorigenesis. The expression ratio of AIMP2-DX2 to normal AIMP2 was increased according to lung cancer stage and showed a positive correlation with the survival of patients. Thus, this work identified an oncogenic splicing variant of a tumor suppressor, AIMP2/p38, and suggests its potential for anti-cancer target.

Citation: Choi JW, Kim DG, Lee A-E, Kim HR, Lee JY, et al. (2011) Cancer-Associated Splicing Variant of Tumor Suppressor AIMP2/p38: Pathological Implication in Tumorigenesis. PLoS Genet 7(3): e1001351. doi:10.1371/journal.pgen.1001351

Editor: Bruce E. Clurman, Fred Hutchinson Cancer Research Center, United States of America

Received September 13, 2010; **Accepted** February 23, 2011; **Published** March 31, 2011

Funding: This work was supported by the Global Frontier (NRF-M1AXA002-2010-0029785), Acceleration Research (R17-2007-020-01000-0), and 21st Frontier Functional Proteomics Research (M108KM010027-08K1301-02710) grants of National Research Foundation funded by the Ministry of Education, Science, and Technology of Korea. The funders had no role in study design, data collection and analysis, decision to publish, or preparation of the manuscript.

Competing Interests: The authors have declared that no competing interests exist.

* E-mail: sungkim@snu.ac.kr

Introduction

Alternative splicing is implicated in the regulation of gene function and diversification [1–3]. Although this process can provide another level of flexibility in gene regulation, the disruption in the balance between splicing variants or the generation of aberrant alternative splicing variants can lead to pathological disorder. In this context, the discovery of aberrant splicing variants that are related to human diseases and the understanding of their mode of action would provide important insights into diagnosis and therapy of the related diseases. In this work, we identified a splicing variant of tumor suppressor, AIMP2, that is associated with cancer formation and characterized its working mechanism and pathological implication.

Nine different aminoacyl-tRNA synthetases (ARSs) form a macromolecular complex with three auxiliary factors, AIMP1, 2, and 3. Many of the enzyme components were previously shown to be involved in diverse signaling pathways with their unique mechanisms [4,5]. The three AIMPs appear to facilitate the assembly of the whole complex through the interactions with each other as well as with their specific target enzymes [6]. These factors also play diverse regulatory roles. AIMP1/p43 is secreted as a cytokine controlling angiogenesis [7], immune response [8,9], tissue regeneration [10] and as a hormone for glucose homeostasis [11]. It is also implicated in the regulation of the autoimmune phenotype such as lupus [12]. AIMP3/p18 was demonstrated to be a tumor suppressor responding to DNA damage [13,14] or oncogenic stimuli [15].

AIMP2 plays a pivotal role in the control of cell fate. It shows anti-proliferative activity by enhancing the growth-arresting signal of TGF-β signal [16]. AIMP2 also promotes cell death via the activation of p53 [17] and apoptotic signal of TNF-α [18]. For this reason, mice lacking AIMP2 were neo-natal lethal due to lung failure resulted from overproliferation of lung epithelial cells. In addition, the AIMP2 heterozygous mice with reduced expression level of AIMP2 showed a higher susceptibility to tumorigenesis [19]. Based on these results, AIMP2 is considered as a haploinsufficient tumor suppressor with unique working mecha-

Author Summary

Lung cancer is one of the most common cancers and a leading cause of death resulting from cancer. Despite intensive investigation, effective therapeutic targets and reliable biomarkers are still limited. Here we found that a tumor suppressor, AIMP2 (MSC p38), produces a variant lacking a part of its structure in cancer tissues. We designated it AIMP2-DX2. This smaller version of AIMP2 compromises the normal tumor suppressive activity of AIMP2 and induces tumor formation. We also found that the expression of AIMP2-DX2 was increased according to cancer progression. In addition, the patients with higher expression of AIMP2-DX2 showed lower survival than those with lower levels of this variant. Suppression of AIMP2-DX2 slowed tumor growth, suggesting it as a new therapeutic target. In summary, this work newly identified a tumor-inducing factor, AIMP2-DX2, that can be used as a therapeutic target and biomarker associated with lung cancer.

nism. Here we identified a splicing variant of AIMP2 that can compromise the normal function of AIMP2 and induce tumorigenesis.

Results

Cancer-associated generation of exon 2–deleted splicing variant

The gene encoding AIMP2 is located in chromosome 7 and consists of four exons (Figure 1A). Interestingly, the expressions of its splicing variant lacking exon 2 (encoding 69aa) was reported in the EST database for cervical carcinoma (BI259092) and muscle rhabdomyosarcoma (BI115365). We designated this variant AIMP2-DX2. To see whether the generation of this variant has any association with cancer formation, we compared the expression of AIMP2-full length and –DX2 with normal and lung cancer cells by RT-PCR. With the primers, JTV-13 and 11 (Figure 1A top and Figure S1), two PCR products were apparently generated in lung cancer cell lines (Figure 1B top). Isolation and sequencing of the two products determined that the upper and lower bands resulted from the full-length (AIMP2-F) and exon 2-deleted (AIMP2-DX2) transcripts, respectively. RT-PCR with the primer, DX2-S2, which is specific to the junction of exon 1 and 3, and JTV5 (Figure 1A and Figure S1) generated the PCR product of the expected size (27.8kD/756 bp) at higher levels in lung cancer cell lines compared with normal cells (Figure 1B middle).

To see whether the increased expression of AIMP2-DX2 is also observed in human cancer tissues, we isolated the cancer regions from different types of human lung cancer patients and compared the AIMP2-F and –DX2 by RT-PCR. In many of the clinical tissues, the AIMP2-DX2 expression was increased in cancerous regions compared to the normal regions (Figure 1C). To further evaluate the higher expression of AIMP2-DX2, we compared the AIMP2-F and –DX2 expressions in adenocarcinoma of human lung cancer using the poly-A polymerase alpha (POPOLA) gene as a reference [20] using quantitative RT-PCR. The expression ratio of AIMP2-DX2 to PAPOLA, was increased to 0.32 in the cancer region compared to 0.14 in the normal region. In contrast, the ratio of AIMP2-F expression to PAPOLA was only slightly increased in cancer region (Figure 1D).

To confirm the identity of the two forms of AIMP2, we introduced each of pcDNA3.1 plasmid encoding mouse AIMP2-F or –DX2 into AIMP2-deficient mouse embryonic fibroblasts

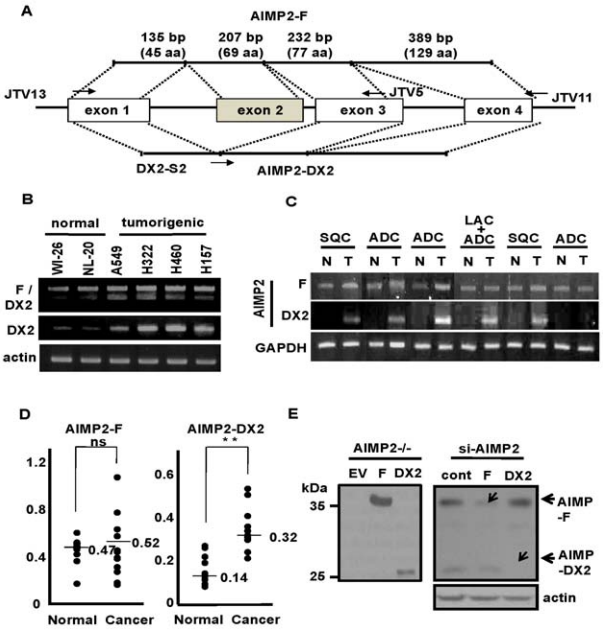

Figure 1. Generation of AIMP2 splicing variant lacking exon 2. (A) The AIMP2/p38 structural gene consists of four exons encoding a total of 320 aa (NM_006303) with three introns. The 312 aa version of AIMP2 is also reported as U24169. Both forms appear to work similarly for most of our experiments although we do not know the reason for the existence of the two forms at this point. The sequences of exon 1, 2 and 3, and the primers, JTV13, JTV5, JTV11 and DX2-S2 are shown in Figure S1. (B) Expression of AIMP2-F and –DX2 was examined in different lung cells (Normal: WI-26, NL-20; tumorigenic: A549, H322, H460 and H157) by RT-PCR using their specific primers shown above. The pair of the primers, JTV13 and JTV11, generates the two PCR products, one from the transcript of AIMP2-full length (upper band) and the other from the exon 2-lacking transcript (lower band). RT-PCR with the primers, DX2-S2, (specific to the junction site of exon 1 and 3, Figure S1) and JTV5, generates the amplicon only from AIMP2-DX2 transcript. Actin was used as the control. (C) Expression of AIMP2-F and AIMP2-DX2 was also determined in different types of human lung cancer tissues and their normal counterparts by RT-PCR. The primer pairs of JTV-13/JTV-5, and DX2-S2/JTV-5 were used for RT-PCR of AIMP2-F and –DX2, respectively. (D) The expression of AIMP2-F and –DX2 were determined in adenocarcinoma (n = 14) and normal (n = 11) lung tissues by quantitative real-time RT-PCR. The cancer regions were obtained by laser microdissection system from archival formalin-fixed paraffin-embedded (FFPE) patient tissues for RT-PCR as described in experimental procedures. PAPOLA [41] was chosen as the endogenous reference gene for quantitative RT-PCR. The expression results were analyzed by Mann-Whitney test and statistical analyses were achieved using SPSS software (SPSS, Chicago, IL). Each dot represents the expression values of AIMP2-F and -DX2 calibrated to the expression level of PAPOLA. The mean values are shown as lines. **, $P<0.01$ (E) The larger and smaller amplicons that were generated by RT-PCR with the primers JTV13 and JTV11 were cloned and expressed in AIMP2-deficient MEFs and their expression was determined by Western blotting with monoclonal anti-AIMP2 antibody (#324) that recognizes both forms of AIMP2. Small interference RNAs targeting AIMP2-F and –DX2 were designed and introduced into A549 cells, and their specific effect on the expression of the corresponding transcripts was determined by Western blotting with anti-AIMP2 antibody (right panel).
doi:10.1371/journal.pgen.1001351.g001

(MEFs) and each transfectant was subjected to Western blotting with AIMP2 antibody, which can recognize both AIMP2-F and –DX2. When proteins were extracted from the transfectants and subjected to immunoblotting with the anti-AIMP2 antibody, AIMP2-F and –DX2-transfected cells showed specific bands at the location of expected molecular weight while no signal was

observed from the EV-transfected cells (Figure 1E left). We also introduced siRNAs designed to specifically target either AIMP2-F or –DX2 into A549 cells in order to validate the identity of the two forms. Each siRNA specifically suppressed the expression of AIMP2-F and –DX2 as expected (Figure 1E right), further confirming the identity of the two transcripts.

Carcinogen-induced mutation increases AIMP2-DX2 level

To see whether the expression of AIMP2-DX2 can be induced by carcinogenic stress, we treated the WI-26 normal lung cells with chemical carcinogen, anti-benzo[*a*]pyrene-7,8-dihydrodiol-9,10-epoxide (BPDE), and selected the surviving cells. We then compared the expression levels of AIMP2-DX2 between the normal WI-26 and surviving cells by Western blotting. The surviving cells expressed higher levels of AIMP2-DX2 compared to that of the normal cells (Figure 2A), suggesting that AIMP2-DX2 can be induced by carcinogenic stress. To determine whether the increased expression of AIMP2-DX2 involves any mutations that might affect alternative splicing pattern between AIMP2-F and –DX2, we isolated the genomic DNA encoding AIMP2 from the surviving cells. We determined the DNA sequences and identified a C39 deletion mutation and a base substitution of A152 to G in exon 2. Furthermore there were substitutions of C227 to T and A342 to G in intron 3 (Figure S2).

We then employed the plasmid (pGINT) containing a splicing cassette that can monitor the alternative splicing by the expression of GFP in 293 cells [21] (Figure 2B). The 1263 base genomic fragment spanning intron 1 (630 bp from 3′end), exon 2 (207 bp) and intron 2 (426 bp from 5′end) of AIMP2 was inserted into the gene encoding GFP (pGINT-exon 2) (Figure 2C). If the exon 2 of AIMP2 is included in splicing, it will be inserted into the middle of GFP, thereby ablating green fluorescence. If exon 2 is skipped during splicing, the normal GFP will be expressed and the cells will generate green fluorescence. To see whether this system would work as expected, pGINT or pGINT-exon 2 was transfected into 293 cells with pRINT that expresses RFP in the same splicing cassette as a control. In both transfectants, RFP was expressed to similar degree, indicating that splicing process occurred normally. In contrast, the transfectants of pGINT-exon 2 showed significantly reduced green fluorescence compared with the pGINT transfectants (Figure 2D). This indicates that splicing process including exon 2 of AIMP2 mainly takes place.

We then introduced pGINT containing the exon 2 insert with different mutations and determined whether any of these mutations induced exon 2 deletion during splicing. Among the transfectants of four tested mutations, the cells containing A152G substitution expressed GFP to the level similar to pGINT control. In control, the cells with three other mutations showed the reduced GFP levels as pGINT-exon 2 wild type (Figure 2E). The effect of the four mutations on exon 2 splicing was also determined by RT-PCR of pGINT-exon 2 constructs. Among the four tested mutant sequences, the DNA containing A152G substitution induced exon 2 skipping and mainly generated GFP transcript whereas the three other mutants generated the transcript like the wild type DNA (Figure 2F).

To identify splicing factors involved in this process, exonic splicing enhancer (ESE) finder program ver. 3.0 [22,23] was used for the serine/arginine-rich (SR) protein-binding motif analysis in exon 2. Motif sequences for the SR proteins, SF2/ASF, SC35, SRp40 and SRp55, were used for the ESE finding and the mutation sites located in exon 2, ΔC39 and A152G, were predicted to be located in the ESEs for SF2/ASF (Figure S3A). Since A152G mutation which induced exon 2 skipping was

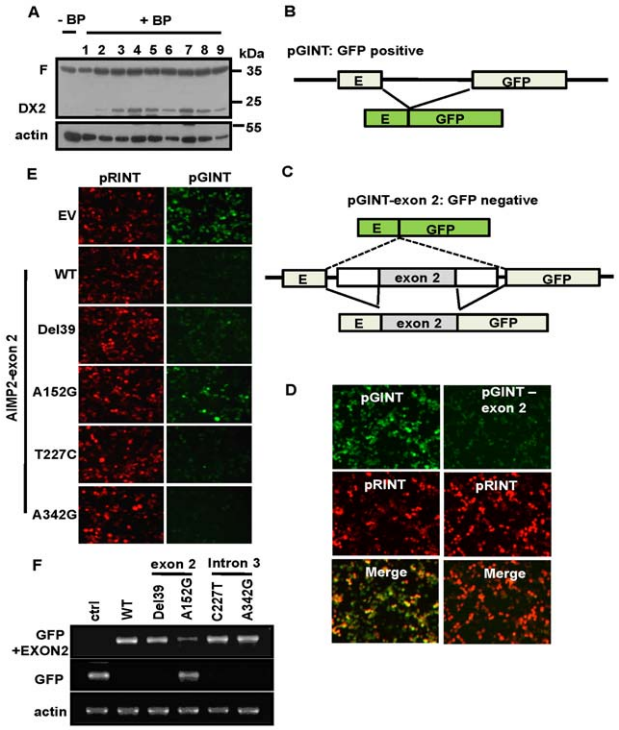

Figure 2. Splicing variant of AIMP2 is increased by carcinogen-induced mutation. (A) Normal lung WI-26 cells were incubated in the presence of BPDE for 4 weeks. The surviving colonies were isolated and further cultivated for additional 2 weeks after removal of BPDE to establish stable cell lines. The expression of AIMP2-F and –DX2 in each isolated cell line was determined by Western blotting with anti-AIMP2 antibody. (B) Schematic representation of the EGFP reporter cassette that monitors alternative splicing in cells (pGINT) [21]. Normal splicing process would delete the intervening DNA sequence that is inserted into the open reading frame of EGFP to restore the expression of EGFP. (C) The intervening sequence is inserted into the 146 base position of 717 bp open reading frame of EGFP. The DNA region spanning the 3′ region of intron 1 (630 bp)-exon 2 (207 bp)-intron 2 (426 bp) of AIMP2 was inserted into the open reading frame of EGFP (pGINT-exon 2). If splicing skips exon 2, EGFP will be expressed (upper). However, the normal splicing including exon 2 will break the open reading frame of EGFP (lower). (D) pGINT (left) or pGINT-exon 2 (right) was introduced into HEK293 cells with pRINT (Red fluorescence protein reporter cassette that generates RFP through constitutive splicing intron), and expression of GFP and RFP was observed. (E) pGINT plasmids containing AIMP2 gene with the indicated mutations were tranfected into HEK293 cells and the expression of EGFP was determined. While pGINT empty vector generated EGFP, pGINT containing the wild type exon 2 and flanking intron regions reduced the expression of EGFP. The effect of the indicated mutations on the exon 2 splicing was monitored by the production of EGFP. All the transfectants showed similar degree of RFP, indicating that the difference in EGFP did not result from the variation of transfection efficiency. (F) Expression of the two transcripts (GFP transcripts with and without AIMP2 exon 2 insert) was also determined by RT-PCR.
doi:10.1371/journal.pgen.1001351.g002

predicted to severely affect the potential ESE site for SF2/ASF, we tested the effect of SF2/ASF on the expression level of AIMP2-DX2. Knockdown of SF2/ASF reduced both AIMP2-F and -DX2 (Figure S3B) and overexpression of SF2/ASF increased the both forms (Figure S3C), implying that AIMP2 pre-mRNA is a functional substrate for SF2/ASF-mediated splicing.

To demonstrate the direct interaction between SF2/ASF and exon 2 RNA, exon 2 RNA was detected after co-precipitation with SF2/ASF. The association of SF2/ASF was observed with WT

exon 2, but not with A152G exon 2 RNA (Figure S3D). Direct interaction between SF2/ASF and exon 2 RNA was also tested by incubating SF2/ASF with exon 2 WT or A15G probe. Among the two probes, only the WT exon 2 probe strongly bound to SF2/ASF (Figure S3E). SF2/ASF controls alternative splicing of tumor suppressors and cell cycle regulatory genes and also shows abnormal expression in various cancers including lung carcinoma [24-26]. Although SF2/ASF appears to control the expression of both AIMP2-F and AIMP2-DX2, the expression of the DX2 form seems to be more dependent on the levels of SF2/ASF. Thus, enhanced expression of SF2/ASF would increase the relative ratio of AIMP2-DX2 to AIMP2-F.

AIMP2-DX2 interferes with pro-apoptotic activity of AIMP2

We investigated how AIMP2-F (full length) and -DX2 would affect DNA damage-induced cell death by monitoring the sub-G1 portion of A549 cells. The sub-G1 portion was increased by adriamycin treatment and it was further augmented by the introduction of AIMP2-F (Figure 3A). However, the exogenous addition of AIMP2-DX2 reduced the adriamycin and AIMP2-F-induced sub-G1 portion of cells (Figure 3A). Since AIMP2-F was shown to mediate the apoptotic response of p53 to DNA damage, we monitored how AIMP2-F and –DX2 would affect the expression of the luciferase reporter gene with the promoter, Growth Arrest and DNA Damage 45 (GADD45), under the control of p53. Luciferase activity was increased according to the added amount of AIMP2-F in the presence of adriamycin (Figure 3B). However, adriamycin-induced luciferase activity was decreased by the addition of AIMP2-DX2 in a dose-dependent manner (Figure 3C).

We also tested the effect of AIMP2-F and –DX2 by fluorescence staining of the cells. AIMP2-F and –DX2 were transfected into the immortalized MEF cells as GFP fusion proteins and the cells were treated with DNA damaging agent, etoposide, for 8 h and the effects of the two proteins on cell death were monitored by cell morphology change using bright field and fluorescence microscopy. The cells expressing GFP-AIMP2-F showed apoptotic morphology with high frequency while other cells still maintained normal shape (Figure 3D). The cells transfected with GFP-AIMP2-DX2 was observed in 16 h after etoposide treatment. Many cells turned to apoptotic morphology as shown by light microscopy whereas most of the GFP-AIMP2-DX2 expressing cells kept normal morphology (Figure 3E). All of these results further confirmed pro-apoptotic activity of AIMP2-F and suggested that AIMP2-DX2 may render resistance to cell death, perhaps by interfering with the normal activity of AIMP2-F.

AIMP2–DX2 blocks pro-apoptotic interaction of AIMP2-F with p53

Since AIMP2-F mediates the apoptotic response to DNA damage via p53, we investigated whether AIMP2-DX2 would influence the pro-apoptotic interaction of AIMP2-F with p53. To see this possibility, we first tested whether AIMP2-DX2 could bind to p53 like AIMP2-F. We transfected the two forms of AIMP2 into A549 cells. The endogenous p53 was immunoprecipitated and the co-precipitation of AIMP2-F or –DX2 with p53 was determined by Western blotting. Both of AIMP2-F and –DX2 were bound to p53 with a similar affinity (Figure 4A). We then prepared radioactive AIMP2-F and DX2 by *in vitro* translation and each protein was mixed with GST or GST-p53. GST-p53 was precipitated with glutathione-Sepharose and co-precipitation of AIMP2-F and –DX2 was determined by autoradiography. Both

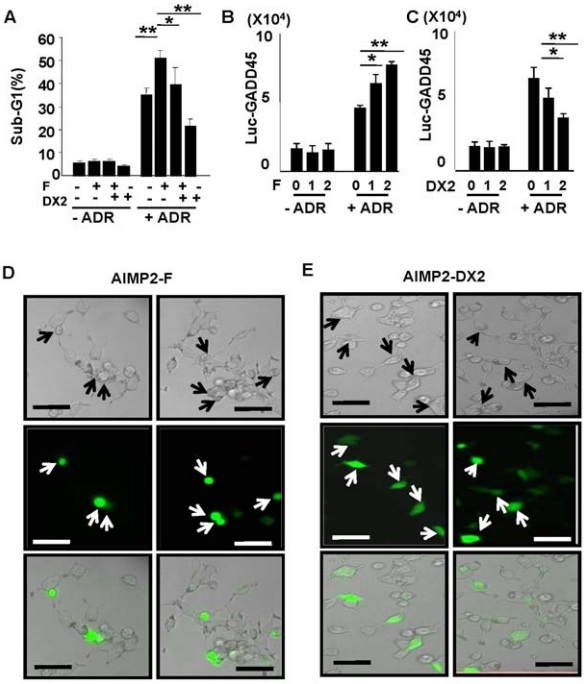

Figure 3. AIMP2-DX2 compromises pro-apoptotic activity of AIMP2-F. (A) AIMP2-F and –DX2 were transfected into A549 cells and their effects on adriamycin-induced cell death were compared by sub-G1 population using flow cytometry. *: $P<0.05$. **: $P<0.01$. A549 cells were transfected with luciferase reporter gene under the control of GADD45 promoter with the indicated amounts of AIMP2-F (B) or AIMP2-DX2 (C), and incubated for additional 12 hours. Adriamycin was treated to the transfectants for 12 hours and luciferase activity was measured by luminometer. (D) MEF cells were transfected with pcDNA3.1 vector and selected by G418 for 2 weeks to establish immortalized cell line. The cells were then transfected with pEGFP-C2 plasmid expressing AIMP2-F. After 24 h, VP-16 (10 μM, Sigma) was added on the dishes and the cells were cultivated for 8 h and the cell morphology was monitored by bright field and fluorescence (489 nm excitation/509 nm emission) microscopy. The images were converged by Metamorph 7.0 imaging program. Bar, 20 μm. (E) EGFP-fused AIMP2-DX2 was also expressed in the same cells and cell morphology was examined in 16 h after VP-16 treatment. Bar, 20 μm.
doi:10.1371/journal.pgen.1001351.g003

proteins were precipitated with GST-p53 but not with GST, further confirming their ability to bind p53 (Figure 4B).

We then investigated whether AIMP2-DX2 would compete with AIMP2-F for the interaction with p53 by *in vitro* pull-down assay using GST-p53 and radioactively synthesized AIMP2-F or –DX2. The binding of AIMP2-F to p53 was decreased by the addition of AIMP2-DX2 in dose-dependent manner (Figure 4C). Conversely, AIMP2-F decreased the binding of AIMP2-DX2 to p53 (Figure 4D). These results confirmed that the two forms of AIMP2 would compete for the binding to p53. Since AIMP2-F can block the interaction between p53 and MDM2 [17], we examined how AIMP2-DX2 would affect the interaction between p53 and MDM2. We added different amounts of AIMP2-F and –DX2 to the binding mixture of radioactive MDM2 and GST-p53, and checked how they would influence the association of p53 and MDM2. While MDM2 binding to p53 was decreased as more AIMP2-F was added (Figure 4E), the addition of AIMP2-DX2 gave no inhibitory effect on the p53-MDM2 association (Figure 4F). These results suggest that AIMP2-DX2 does not block MDM2 binding to p53. We then examined the binding of AIMP2-F and –DX2 to p53 at endogenous levels. In normal lung WI-26 cells, we

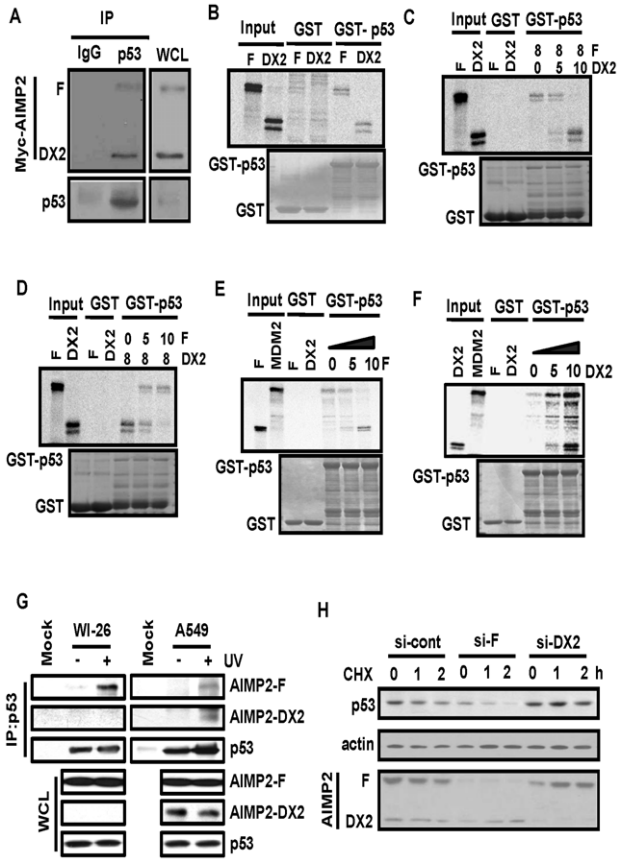

Figure 4. The effect of AIMP2-DX2 on the interaction of AIMP2-F with p53. (A) p53 was immunoprecipitated from A549 cells transfected with Myc-AIMP2-F and –DX2, and co-precipitation of the two AIMP2 proteins with p53 was determined with anti-Myc antibody. (B) AIMP2-F and –DX2 were radioactively synthesized by *in vitro* translation and each protein (20 μl of the *in vitro* translation reaction) was mixed with GST or GST-p53. GST proteins were precipitated with glutathione-Sepharose beads and co-precipitation of AIMP2-F and –DX2 was determined by autoradiography. (C) Radioactively synthesized AIMP2-F and –DX2 as above were used to see whether the two proteins would compete for the interaction with p53. The indicated amount of AIMP2-DX2 (indicated by microliter volume) was mixed with the fixed amount of AIMP2-F and GST-p53 to see the effect of AIMP2-DX2 on the AIMP2-F binding to p53. (D) Conversely, the indicated amount of AIMP2-F was added to the fixed amount of AIMP2-DX2. (E) MDM2, AIMP2-F and –DX2 were radioactively synthesized as above and the indicated volumes (μl) of AIMP2-F was added to the binding mixture of MDM2 and GST-p53. The mixture was precipitated with glutathione-Sepharose and co-precipitation of MDM2 and AIMP2-F was determined by autoradiography. (F) The same experiment as above was conducted except that AIMP2-DX2 was added at the indicated amounts to the mixture. (G) WI-26 and A549 cells were subjected to UV irradiation and lysed. The extracted proteins were immunoprecipitated with anti-p53 antibody (FL-393), separated by SDS-PAGE and immunoblotted by immunoblotting with the anti-AIMP2 antibody. (H) A549 cells were treated with cycloheximide (CHX) to block *de novo* protein synthesis. AIMP2-F and –DX2 were suppressed with their specific siRNAs and the cellular levels of p53 were monitored by Western blotting at indicated time interval.
doi:10.1371/journal.pgen.1001351.g004

observed UV-dependent association of AIMP2-F with p53 (Figure 4G left). However, in lung cancer A549 cells expressing higher level of AIMP2-DX2, endogenous AIMP2-DX2 bound to p53 to the extent similar to AIMP2-F, further supporting the potential competition between the two forms of AIMP2 for the binding to p53 (Figure 4G right).

We next compared the effect of AIMP2-F and –DX2 on the cellular stability of p53 after knocking down AIMP2-F and –DX2. A549 cells were treated with cycloheximide (CHX) to block the *de novo* cellular protein synthesis, and AIMP2-F or –DX2 was specifically suppressed with their specific siRNAs. Then, the cells were harvested at time intervals and the cellular levels of p53 were determined by Western blot analysis. When AIMP2-F was suppressed, the cellular level of p53 was more rapidly reduced compared with that of the si-control-treated cells. In contrast, the level of p53 was maintained for longer duration in the cells in which AIMP2-DX2 was suppressed with its specific siRNA (Figure 4H). This property means that AIMP2-DX2 would work like a dominant negative mutant against the pro-apoptotic interaction of AIMP2-F with p53. For this reason, cells showed an increased sensitivity to etoposide-induced cell death when endogenous AIMP2-DX2 was suppressed, (Figure S4A), and this increased sensitivity was abrogated in p53-deficient cells (Figure S4B), indicating that the effect of AIMP2-DX2 involves p53.

AIMP2-DX2 stays as free form

Although AIMP2-DX2 expression can be induced, the total amount of AIMP2-DX2 appears to be much lower than that of AIMP2-F in most of the cell lines. This observation poses the question whether AIMP2-DX2 could effectively compete with AIMP2-F for the binding to p53. In this regard, it should be noted that AIMP2-F is mainly anchored to the multisynthetase complex in cytosol [6]. In other words, only a portion of AIMP2-F is recruited to p53 upon DNA damage while the majority of AIMP2-F is still bound to the complex [17]. We checked whether AIMP2-DX2 would also bind to the multi-synthetase complex like AIMP2-F by yeast two hybrid assay. KRS (lysyl-tRNA synthetase), one of the components for the multisynthetase complex, was used as the testing pair for AIMP2-F and –DX2 because AIMP2 make a strong binding to KRS [6,27]. Although AIMP2-DX2 showed the binding ability to p53 with a similar affinity to AIMP2-F, it lost the normal affinity to KRS as determined by yeast two hybrid assay (Figure 5A). This result was further confirmed by co-immunoprecipitation assay. When Myc-AIMP2-F or –DX2 was immunoprecipitated in 293 cells, KRS was co-precipitated with AIMP2-F, but not with –DX2 (Figure 5B). Conversely, when KRS was immunoprecipitated, co-precipitation of AIMP2–DX2 was significantly lower than that of AIMP2-F (Figure 5C).

We also compared the cellular levels of AIMP2-F and –DX2 that exist unbound to the multisynthetase complex. This time, we used AIMP1, another component of the complex [28], instead of KRS, for immunoprecipitation to make sure that we are not looking at only the binary interaction between AIMP2 and KRS. AIMP1 was immunoprecipitated with its specific antibody, and the co-precipitation of AIMP2-F and -DX2 was determined. AIMP2-F, but not AIMP2-DX2, was co-precipitated with AIMP1 (Figure 5D left). We then examined the amounts of AIMP2-F and –DX2 left in the immune-depleted supernatant. The majority of the cellular AIMP2-DX2 was detected in the supernatant that was comparable to the free form of AIMP2-F (Figure 5D right). All of these results suggest that AIMP2-DX2 would exist mainly as free form, not bound to the multisynthetase complex, whereas AIMP2-F is bound to the complex. Thus, AIMP2-DX2 would be able to compete with AIMP2-F that is dissociated from the multisynthetase complex for the binding to p53 and Far-upstream element-binding protein (FBP) although the total amount of AIMP2-DX2 is lower than AIMP2-F (Figure 5E).

Tumorigenic property of AIMP2-DX2

Since AIMP2 works as a potent tumor suppressor, AIMP2-DX2 may exert the opposite activity by interfering with the normal

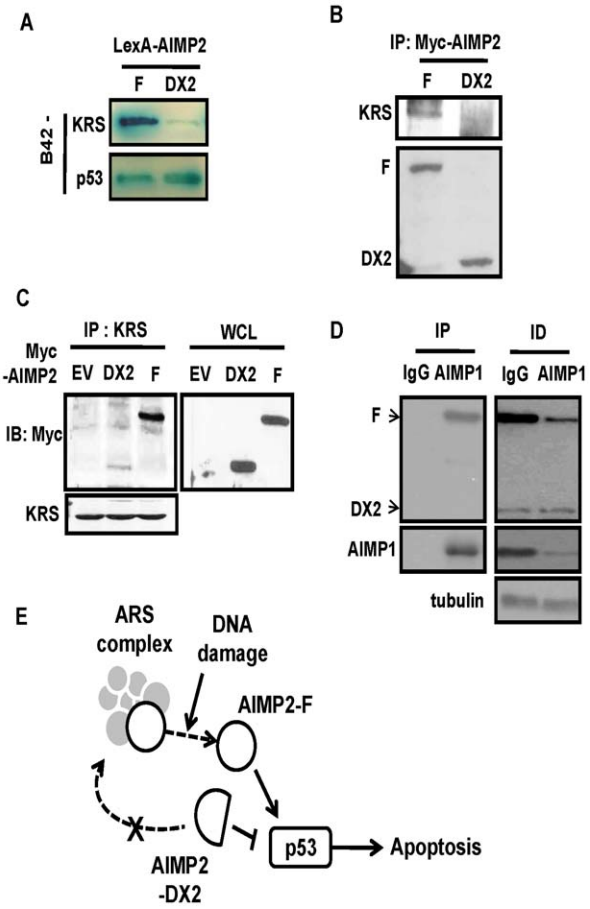

Figure 5. Differential interaction of AIMP2-F and –DX2 with the multisynthetase complex. (A) The interaction of AIMP2-F and –DX2 with the multi-synthetase complex was determined by yeast two hybrid assay using KRS as the target protein. p53 was used as a positive control and the positive interaction was indicated by the blue colony formation on X-gal-containing yeast medium. (B) The interaction of AIMP2-F and –DX2 with KRS was tested by co-immunoprecipitation assay. Myc-AIMP2-F or –DX2 was expressed in 293 cells and immunoprecipitated with anti-Myc antibody. Co-precipitation of KRS was determined with anti-KRS antibody. (C) KRS was immunoprecipitated with its specific antibody and co-precipitation of Myc-AIMP2-F, and –DX2 was determined with anti-Myc antibody. Expression of KRS and Myc-tagged AIMP2 were determined by Western blotting with anti-KRS and -Myc antibodies in the whole cell lysates (WCL), respectively. (D) Protein lysates of A549 cells were immunoprecipitated with anti-AIMP1 antibody, and co-precipitation of AIMP2-F and –DX2 was determined by Western blotting with anti-AIMP2 antibody (left). The immune-depleted supernatants were then subjected to Western blotting with anti-AIMP1 and –AIMP2 antibodies (right). (E) Schematic representation for the working mode of AIMP2-F and –DX2 in p53-mediated apoptosis. Upon DNA damage, AIMP2 in the multisynthetase complex is activated and binds to p53 to protect it from MDM2-mediated degradation. AIMP2-DX2 does not associate with the complex and exists as free form. AIMP2-DX2 competes with AIMP2-F for the binding to p53 and compromises pro-apoptotic activity of AIMP2-F via p53.
doi:10.1371/journal.pgen.1001351.g005

activity of AIMP2. To determine this possibility, we isolated WI-26 cells, in which AIMP2-DX2 expression was induced by BPDE to different degrees, and compared their propensity to anchorage-independent colony formation. The same number of the cells was spread on agar plates and the resulting numbers of colonies were counted. The number of the anchorage-independent colonies showed a positive correlation to the expression levels of AIMP2-DX2 (Figure 6A), implicating the potential oncogenic property of AIMP2-DX2. To further confirm these results, we transfected an empty vector, AIMP2-F and AIMP2-DX2 into MEF, and then performed anchorage-independent colony forming assay. Transfection of AIMP2-F and –DX2 resulted in fewer and more colonies compared to that of empty vector (Figure 6B).

To see whether an increased expression of AIMP2-DX2 may render susceptibility to tumorigenesis, we generated transgenic mice in which AIMP2-DX2 is constitutively expressed, as described in Materials and Methods. The increased expression of AIMP2-DX2 was confirmed by Southern blotting with the primers specific to the junction of exon 1 and 3, and by RT-PCR with the primers specific to CMV transgenic vector (Figure S5). In addition, we compared the expression of AIMP2-DX2 by Western

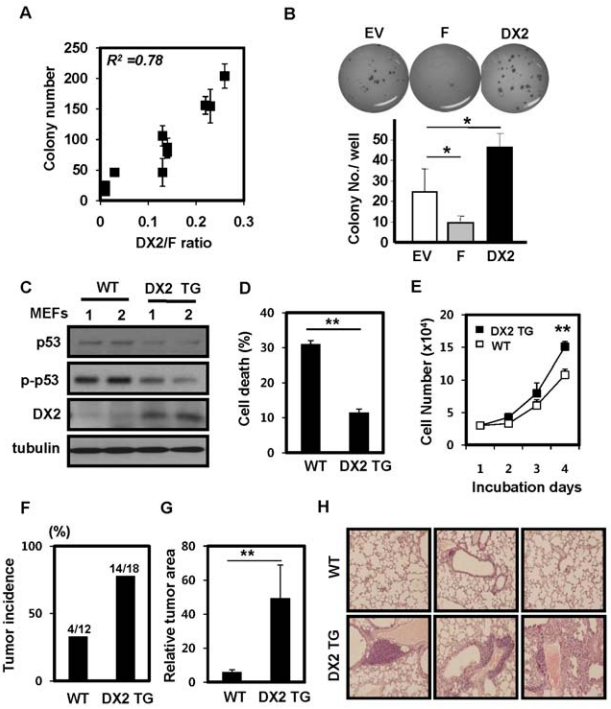

Figure 6. Oncogenic property of AIMP2-DX2. (A) BPDE-transformed WI-26 cells with different expression ratio of AIMP2-DX2 to AIMP2-F were tested for their propensity to anchorage-independent colony formation. The relationship between the ratio of AIMP2-DX2 to AIMP2-F and the average numbers of the produced colonies with standard deviation in each colony were displayed as dot plot. (B) WI-26 cells stably expressing EV, AIMP2-F and -DX2 were also compared for anchorage-independent colony formation. The same numbers of the three cell lines (200 cells per plate) were spread on the testing medium and the resulting colonies were counted and shown as bar graph. The experiments were repeated three times. (C) Two independent 12.5d MEFs were obtained from the wild type and AIMP2-DX2 transgenic mice and compared for the expression levels of p53 and phosphorylation status of p53. Expression of AIMP2-DX2 was also determined by Western blot analysis. Tubulin was used as a loading control. 12.5d MEFs isolated from the wild type and AIMP2-DX2 transgenic mice were treated with adriamycin (1 μM) for 24 h and the sub-G1 populations induced by adriamycin treatment were determined by flow cytometry (D). The cell growth in completed media was also monitored (E). Susceptibility to benzopyrene-induced lung carcinogenesis was compared between the wild type and AIMP2-DX2 transgenic mice by tumor incidence (F) and area (G). The area was represented by the numbers given in Bio-Image J 2.0. (H) Three lungs were isolated from the wild type and AIMP2-DX2 transgenic mice and subjected to hematoxylin and eosin staining.
doi:10.1371/journal.pgen.1001351.g006

blotting and found that AIMP2-DX2 is highly expressed in the transgenic mice (Figure S5). We isolated MEFs from the wild type and AIMP2-DX2 transgenic mice and compared the cellular levels of p53 and its phosphorylation. The p53 level and phosphorylation were significantly reduced in the transgenic mice (Figure 6C). Normal and AIMP2-DX2 MEFs were also treated with adriamycin and their sensitivity to cell death was compared by flow cytometry. AIMP2-DX2 transgenic cells showed lower cell death (Figure 6D), resulting in the enhanced cell number (Figure 6E) compared to the wild type cells. The wild type (n = 14) and AIMP2-DX2 transgenic mice (n = 18) were also compared for their susceptibility to benzo[a]pyrene-induced lung carcinogenesis. Lungs were isolated and the formation of lung cancers were determined as described previously [19] and tumor area was analyzed by Bio-Image J 2.0. The AIMP2-DX2 transgenic mice showed a significant increase in tumor incidence and regions compared to the wild type counterpart (Figure 6F, 6G and 6H). All of these results suggest the oncogenic potential of AIMP2-DX2.

Suppression of AIMP2-DX2 reduces tumor growth

To see whether we can control tumor progression by suppressing the expression of AIMP2-DX2, we established a lung cancer xenograft model with the lung cancer cell line, H460. We introduced siRNA against AIMP2-DX2 and siRNA control via intratumoral injection four times at three day interval from 5 days after cell transplantation. The tumor growth was retarded by the injection of si-DX2 (Figure 7A). We isolated the tumors and compared the expression levels of p53. The tissues isolated from the si-DX2-injected tumors showed higher expression of p53 (Figure 7B), indicating that the si-DX2-injected tumors may have enhanced cell death through the activation of p53. We also determined whether intratumoral injection of si-DX2 actually reduced the expression level of AIMP2-DX2 in tumor region by quantitative real-time PCR. The cellular levels of AIMP2-DX2 were reduced about 50% by the introduction of si-DX2 compared to those in the siRNA control-injected tumors (Figure 7C). For an additional experiment, we introduced luciferase-expressing A549 lung cancer cells into the mice via tail vein. After 2 months of cancer cell inoculation, siRNA control and si-DX2 were delivered to the lungs via intubation four times in three day interval and the mice were incubated another 2 weeks. The lung cancer cell growth was monitored by the luciferase activity released from the growing cancer cells. While the control siRNA-injected mice (n = 5) showed a 2.4 to 4.8 fold increase in luciferase activity, si-DX2-delivered mice showed 1.1 to 2.8 fold increase or even a shrinkage of tumors (Figure 7D). We also isolated the lungs and compared the tumor area by histological analysis. Compared to the siRNA control-delivered tumors, si-DX2-delivered tumors showed smaller cancer regions (Figure 7E). Specific suppression of AIMP2-DX2 transcript was also confirmed by quantitative RT-PCR (Figure S6). Next, we monitored the effect of AIMP2-DX2 suppression on tumor growth using a carcinogen-induced lung cancer model. Lung cancer in mice was induced by the injection of benzo[a]-pyrene (B[*a*]P). Then, we prepared the plasmid DNA encoding shRNA targeted against AIMP2-DX2, and delivered it into lungs via inhalation device eight times in three day interval (Figure S7). We isolated the lungs from the EV- and sh-DX2 treated mice and compared the tumor growth by H&E staining. The DX2-shRNA treated lungs contained smaller tumor area compared to those treated with an empty vector (Figure 7F, 7G and Figure S8). To assure that the plasmid is efficiently delivered to various lung tissues, the same plasmid encoding GFP was prepared and delivered to lung using the same method. The lungs were isolated from the treated mice and the delivery of the plasmid was monitored by the expression of GFP (Figure S8A and S8B). Delivery of sh-DX2 from the treated lungs was confirmed by PCR (Figure S8C). All of these results consistently demonstrated that suppression of AIMP2-DX2 expression can retard tumor growth.

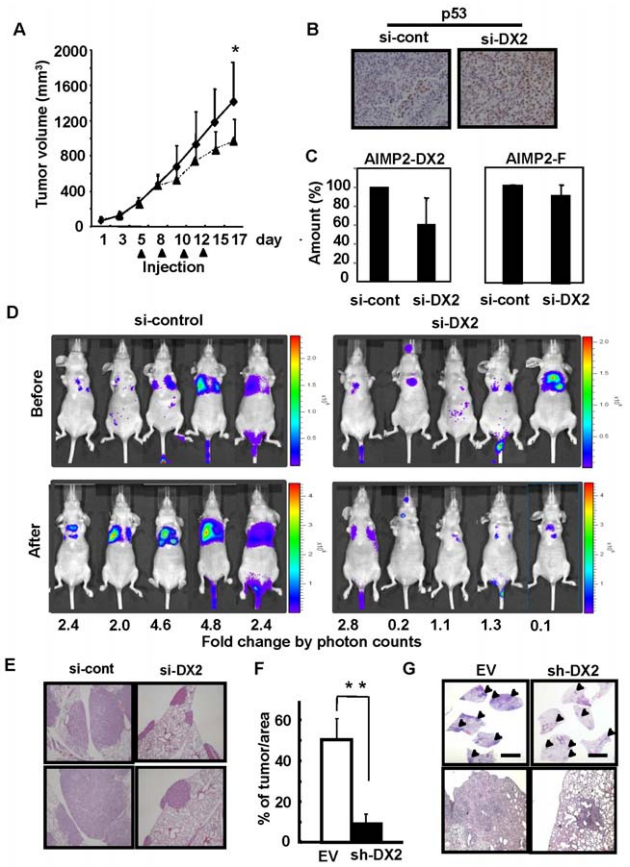

Figure 7. Knock-down of AIMP2-DX2 can retard tumor growth. (A) NCI-H460 (1×10^7) cells were injected at both flanks of 6 week old BALB/c nude mice. When volume of tumor mass reached to 250 mm^3, anti-DX2 or control siRNAs were intratumorally injected at 50 mg/kg dosage once in three days for four times (n = 7 per each group). The tumor volumes were determined as described in Materials and Methods. (B) Tumors isolated from anti-DX2 and control siRNA treated mice were subjected to immunohistochemistry with the antibodies against p53 (C) Cellular levels of AIMP2-F and –DX2 transcripts in the tissues of the isolated tumors were compared by quantitative RT-PCR. (D) Luciferase-expressing A549 lung cancer cells (1×10^7) were injected into tail vein of BALB/c nude mice and the dissemination of the cells into lungs was monitored by IVIS (Xenogen). Each group of the injected mice (n = 5/group) intratracheally received si-scramble (50 μg) or si-AIMP2-DX2 (50 μg) mixed with GDM-PEI in 50 μl of 0.9% saline. The tumor growth was monitored by photon flux released from luciferin as described in Materials and Methods. The data were expressed as photon-flux (photons/s/cm2/steradian). The photon flux for each measurement is represented by color scale. (E) Tumor tissues isolated from each group were examined by hetatoxylin and eosin staining. Two examples from each group are displayed. (F) The plasmid DNA encoding shRNA against AIMP2-DX2 was mixed with glucosylated polyethyleneimine (G-PEI), vaporized in humid vacuum chamber and inhaled for 30 minutes through the nose of the mice that contained benzopyrene-induced lung cancers as described in Materials and Methods. The mice were randomly sacrificed at time interval and the tumor growth was determined by the area of tumor tissues in the total measured area (n = 4). (G) Histological analysis of tumor regions by hematoxylin and eosin staining. Arrow heads indicate tumor nodules.
doi:10.1371/journal.pgen.1001351.g007

Correlation of AIMP2-DX2 expression with cancer stage and patient survival

Since AIMP2-DX2 compromises tumor suppressive activity of AIMP2-F via competitive inhibition, the expression ratio of AIMP2-DX2 to AIMP2-F may have a relationship to cancer progression. To explore this possibility, we obtained squamous cell carcinoma and adenocarcinoma tissues from lung cancer patients who were in different stages, and the expression ratios of AIMP2-DX2 to -F were compared. The AIMP2-DX2/F ratios were gradually increased from those of the normal tissues according to cancer stage (Figure 8A).

We also determined the expression of AIMP2-DX2 and AIMP2-F in the normal and cancerous regions isolated from 97 NSCLC patients by quantitative RT-PCR. The patients were divided into two groups based on the expression ratios of AIMP2-DX2 to AIMP2-F. 43 patients showed higher expression ratios of AIMP2-DX2 to AIMP2-F in cancerous regions compared with those in the normal regions while the other 54 patients did not show apparent difference between the cancer and normal tissues. The patient group with tumors that expressed higher ratios of AIMP2-DX2 to AIMP2-F exhibited a poorer overall (Figure 8B) and disease-free survival (Figure 8C) pattern compared to the group in which the patients did not show higher expression of AIMP2-DX2 although the degree of difference between the two groups varied to some extent. When we examined the prognostic values with several factors, the AIMP2-DX2 to AIMP2-F expression ratio showed the most significant correlation with patient survival (Table 1, Table S1, Hazard Ratio for Overall Survival $=6.83$, $P=0.045$; Hazard Ratio for Disease Free Survival $=2.25$, $P=0.046$). Altogether, the results further support that increased expression of AIMP2-DX2 may reflect the aggressiveness of cancer cells.

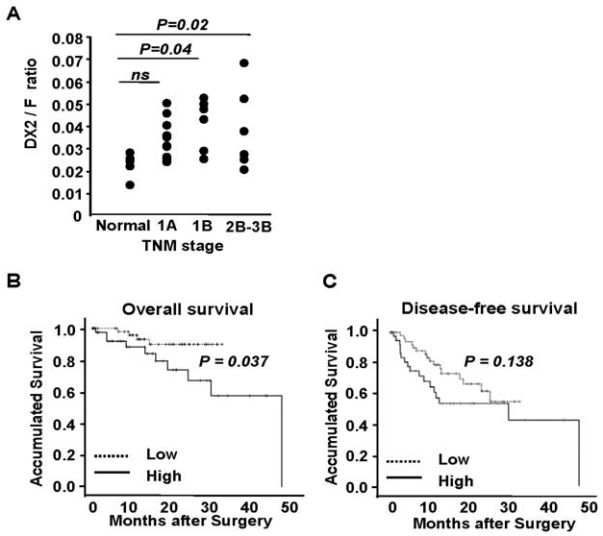

Figure 8. Correlation of expression ratio of AIMP2-DX2 to AIMP2-F with lung cancer stage and survival. (A) AIMP2-DX2/F ratios of patient tissues with cancer stage IA (n = 5), IB (n = 6) and IIB~IIIB (n = 7) were compared with that of normal lung tissues (n = 5) by quantitative RT-PCR method as described. The ratios were increased significantly *($p<0.05$)* according to tumor progression. Cancer stages were classified based on TNM (tumor, nodes, metastasis) system. Kaplan-Meier estimates of the (B) OS and (C) DFS according to the level of the expression ratios of AIMP2-DX2 to AIMP2-F in 97 lung cancer patients. The OS was significantly worse in patients with higher expression ratio of AIMP2-DX2 to AIMP2-F than in patients with lower expression ratio. *P*- values were calculated by the log-rank test.
doi:10.1371/journal.pgen.1001351.g008

Table 1. Multivariate analysis for overall and disease-free survival by demographics, smoking status, histological type, and pathologic stage.

	Overall Survival		Disease-Free Survival	
Variables	**HR (95% CI)**	***P***	**HR (95% CI)**	***P***
Age (>63/≤63 years)	13.7 (1.36–90.9)	0.03	3.59 (1.42–9.01)	0.01
Gender (Female/Male)	0.91 (0.06–13.9)	0.95	1.04 (0.29–3.68)	0.96
Smoking status (Ever/Never)	0.87(0.10–7.54)	0.90	0.83 (0.23–2.93)	0.77
Histology (AD/SQ)	1.98 (0.35–11.2)	0.44	2.38 (0.76–7.40)	0.13
Stage (II-IIIA/I)	1.40 (0.26–7.57)	0.69	2.60 (1.03–6.57)	0.04
Adjuvant treatment (No/Yes)	2.54 (0.41–15.1)	0.32	1.39 (0.51–3.86)	0.52
DX2 expression (High/Low)	6.83 (1.05–44.5)	0.045	2.55 (1.01–6.42)	0.046

Row percentage shown. HRs, 95% CIs and their corresponding *P*-values were calculated using multivariate Cox proportional hazard models, adjusted for age, gender, smoking status, tumor histology, pathologic stage and adjuvant treatment. *P*-values were statistically significant after Bonferroni correction for multiple testing.
doi:10.1371/journal.pgen.1001351.t001

Discussion

Although alternative splicing can be a way for the diversification of a gene function [1–3], the generation of inappropriate splicing product can be pathologic. In particular, the cancer-associated formation of alternative splicing variants has been reported in prostate cancer [29]. Oncogenic alternative splicing variants of Acute Myeloid Leukemia 1 (AML1) and TrkA have been found in ovarian cancer [30] and neuroblastoma [31], respectively. Similarly, the splicing variant of p53 was also shown to modulate the normal activity of p53 [32,33]. In p63, another p53 family tumor suppressor, a splicing variant expressed dominant negative activity [34–36]. Based on these findings, alternative splicing variants with oncogenic properties are expected to be found in other tumor suppressors. Here we report a generation of an oncogenic alternative splicing variant of tumor suppressor AIMP2 in lung cancer cells and patient tissues (Figure 1).

The base substitution of A152 to G was found at the exon 2 region of AIMP2 in carcinogen-induced transformed cells. This mutation induced exon 2 skipping, resulting in the increase of AIMP2-DX2 production (Figure 2E and 2F). These results further support the association of AIMP2-DX2 with tumorigenesis. Generation of AIMP2-DX2 does not seem to seriously affect the cellular level of AIMP2-F transcript. Perhaps this is because the amount of AIMP2-DX2 is minor compared to that of AIMP2-F or because the loss of AIMP2-F resulting from the generation of AIMP2-DX2 is re-filled by a compensatory expression. Further detailed investigation is needed to see how alternative splicing between AIMP2-F and –DX2 is regulated.

AIMP2-DX2 competes with AIMP2-F for the binding to p53 (Figure 4). In our previous work, deletion mapping determined that the C-terminal region (161–312 aa) of AIMP2 binds to the N-

terminal region of p53 [17]. Thus, it is not surprising that AIMP2-DX2 retains its binding ability to p53 because the exon 2 encodes the region of 46–113 aa of AIMP2, which is not involved in the interaction with p53. Based on the conformational modeling, the exon 2 domain is expected to protrude outward and may give a steric hindrance for MDM2 to bind p53 (data not shown). Since AIMP2-DX2 polypeptide is smaller than AIMP2-F and may not have the expected protuberance of exon 2, it may not be able to block the MDM2 binding to p53.

AIMP2 also plays critical roles in the apoptotic activity of TNF-α [18] and the anti-proliferative activity of TGF-β [16]. Although in this study we focused on the antagonistic function of AIMP2-DX2 against the pro-apoptotic activity of AIMP2-F via p53 in response to DNA damage, it may also influence the normal activity of AIMP2 in these two other pathways with a similar mode of action, namely, through the competitive binding to the target proteins. Since AIMP2-F augments TGF-β-dependent growth arrest via downregulation of FBP and c-Myc [16], we examined whether AIMP2-DX2 would also work against AIMP2-F in this pathway. While overexpression of AIMP2-F increased p53 level, it reduced the levels of FBP and c-Myc (Figure S9A). Exogenous supplementation of AIMP2-DX2 reversed these effects of AIMP2-F (Figure S9A). We also examined the effect of AIMP2-DX2 on the ubiquitination of AIMP2-F target proteins. While p53 ubiquitination was inhibited by AIMP2-F, it was interfered by the addition of AIMP2-DX2 (Figure S9B). Conversely, ubiquitination of FBP was enhanced by the addition of AIMP2-F (Figure S9C) and this effect was inhibited by exogenous introduction of AIMP2-DX2 (Figure S9C). We also compared the expression level of c-Myc as well as p53 among WI-26 and other lung cancer cell lines such as H460, H1975 and H292 (all of these cell lines contain wild type p53) in which AIMP2-DX2 levels are increased. In these cell lines, c-Myc level was more increased compared to that of the normal WI-26 cells while p53 levels were more decreased (Figure S9D). Interestingly, all of these cells lines showed increased SF2/ASF levels, further supporting the regulatory connection between this splicing factor and expression of AIMP2-DX2. Based on these results, AIMP2-DX2 is expected to compromise not only the pro-apoptotic activity but also anti-proliferative activities of AIMP2-F.

Considering the functional importance of AIMP2 in cell fate determination as well as in the assembly of multisynthetase complex [37,38], its cellular level and activity may need to be tightly controlled. For this, expression of AIMP2-DX2 can be a part of a normal regulatory mechanism to finely control the function of AIMP2. Perhaps, the generation of AIMP2-DX2 could become out of control by mutations that can disrupt the normal splicing process and lead to cancer formation. The responsible mutations can be located in *trans*-acting splicing factors or in the promoter or gene encoding AIMP2. Suppression of AIMP2-DX2 in lung cancer reduced tumor growth in lung cancer model (Figure 7), and lung cancer patient analysis demonstrated the correlation of AIMP2-DX2 expression with cancer progression and patient survival (Figure 8). Combined with the molecular working mechanism and cellular effect, AIMP2-DX2 appears to be a novel therapeutic target against lung cancer. It would be interesting to see whether this variant would be also involved in other types of cancer.

Materials and Methods

Cell culture and reagents

Normal lung cell line, WI-26, was purchased from Korea Cell Line Bank (KCLB) and NL-20 was provided by Dr. M.-H. Cho (Seoul National University). Lung carcinoma cell lines A549 and NCI-H460 were obtained from ATCC, and H322 and H157 from KCLB. The siRNAs targeting AIMP2-F and -DX2 were designed as the sequences of AGAGCUUGCAGAG ACAGGUUAGACU and UCAGCGCCCCGUAAUCCUGCACG UG, respectively. AIMP2-DX2 polypeptide was used as the antigen and the selected hybridoma clone (#324) generated the monoclonal antibody recognizing both of AIMP2-F and –DX2. This antibody was used for immunoblotting and immunohistochemistry. Anti-KRS and –AIMP1 antibodies were purchased from Abchem.

Quantitative RT–PCR

The expression of AIMP2-DX2 and –F were analyzed by quantitative real time RT-PCR. Eleven normal lung samples and fourteen patients with lung adenocarcinoma were retrospectively identified from the surgical pathology files of the Department of Pathology at Samsung Medical Center and their archival formalin-fixed paraffin-embedded (FFPE) tissues were obtained. All the samples were collected anonymously according to Institutional Review Board guidelines. All patients had undergone a surgical operation and had received neither chemotherapy nor radiotherapy before surgical resection. For total RNA extraction from FFPE tissues, each tissue section was stained with hematoxylin and cancer regions were microdissected using laser microdissection system (ION LMD, JungWoo International, Korea). Paradise Whole Transcript RT Reagent System (Arcturus, CA, USA) was used for RNA isolation and RT of FFPE samples. Due to the limitation of RNA amount extracted from FFPE tissues, half RNA and cDNA were used for reverse transcription and quantitative RT-PCR, respectively. PCR primers and Taqman probes for this study are provided from Metabion (Germany).

Flow cytometry

Cells transfected with the plasmid encoding AIMP2-F or –DX2 were cultivated in the absence or presence of adriamycin, fixed with 70% ethanol for 1 hour at 4°C and washed with ice-cold PBS two times. Then, the 1×10^6 cells were stained with PI (50 μg/ml) containing 0.1% sodium citrate, 0.3% NP40 and 50 μg/ml RNase A for 40 minutes, and subjected to flow cytometry (FACS Caliber, Beckton-Dickinson) for the determination of apoptotic cells by counting sub-G1 cells. For each sample, 20,000 cells were analyzed using Cell Quest Pro software. All of the experiments were repeated three times and averaged.

Anchorage-independent colony forming assay

pCDNA3 encoding AIMP2-F and -DX2 were transfected into 12.5 days mouse embryonic fibroblasts. The cell lines stably expressing each of the transfected plasmid were established by G418 selection. For soft agar colony assays, the cells were diluted into 0.3% agar in DMEM containing 10% FBS and seeded in triplicate onto 0.6% agar containing culture medium. 200 cells were seeded on each well in 12-well plate. The colonies were fed in every 3 to 4 days and evaluated after 5 weeks. To evaluate the correlation between the expression level of AIMP2-DX2 and colony formation, WI-26 cells (Korean Cell Line Bank) were treated with 0.1 μM BPDE once in every three days for 4 weeks and the surviving colonies were observed after 2 weeks from the chemical treatment. The 20 separate colonies were randomly selected to establish the cell lines.

Binding assay

For immunoprecipitation, AIMP2-F or DX2 was ectopically expressed in HEK293 cells by transfection. The cells were lysed with the lysis buffer containing 1% NP-40, 0.5% deoxycholate and

protease inhibitor cocktail (Calbiochem). The lysates were incubated with the antibody against p53 (DO-1, Santacruz), and precipitated by protein G (Invitrogen) 4°C overnight and co-precipitation of the two proteins were blotted with anti-Myc or anti-AIMP2 antibody. For *in vitro* pull down assay, GST-p53 or GST was mixed the protein extracts with glutathione-Sepharose in the PBS buffer containing 1% Triton X-100 and 0.5% N-laurylsarcosine at 4°C for 2 hours. We synthesized MDM2 and AIMP2-F or -DX2 by *in vitro* translation in the presence of [^{35}S] methionine using TNT Quick coupled Transcription/Translation system (Promega). The synthesized peptide was added to the GST protein mixtures above, incubated at 4°C for 4 hours with rotation in the PBS buffer containing 1% Triton X-100, 0.5% N-laurylsarcosine, 1 mM DTT, 2 mM EDTA and 300 μM phenylmethylsulfonyl fluoride (PMSF), and washed six times with the same buffer containing 0.5% Triton X-100. We then eluted the proteins bound to Sepharose beads with the SDS sample buffer, separated by SDS-PAGE and autoradiographed. For yeast two hybridization assay, the cDNAs encoding human AIMP2-F, –DX2, p53 and KRS were obtained by PCR using specific primers. The PCR products were digested with *Eco*RI and *Xho*I, and ligated into the same sites of pEG202 (LexA) and pJG4-5 (B42). The interactions between LexA-AIMP2 fragments and B42-KRS or –p53 were analyzed for their ability to form blue colonies on yeast medium containing X-gal.

Reporter gene assay

To test the p53-dependent transcriptional activity, the target gene GADD45-luciferase vector was transfected into A549 cells. The cells lysates were prepared and reacted by luciferase assay kit following the manufactuerer's protocol (Promega) and the luciferase activity was analyzed using luminometer.

Mutation analysis for AIMP2-DX2 generation

The 1263 bp genomic DNA of AIMP2 covering exon 2 with flanking introns was amplified with Platinum *Taq* DNA polymerase high fidelity (Invitrogen) and DNA template from BPDE-transformed WI-26 cells (WI-26T) with the primers 5′GAAGAGTCTAACCTGTC TCTGCAAGCTCTTGAG3′ and 5′AACATGCTCTTGGCT CTGCCTTTG3′. The resulting PCR products were cloned into pGEMT-Easy vector (Promega) and sequenced. To verify the effect of mutations in WI-26T cells on AIMP2-DX2 generation, the splicing reporters, pGINT and pRINT, which express EGFP and RFP, respectively as an indication of splicing, were kindly provided by Dr. Garcia-Blanco [21]. The genomic wild type AIMP2 exon 2 regions including *cis*-acting splicing elements were amplified with Platinum *Taq* DNA Polymerase High Fidelity (Invitrogen) using primers (5′GCGCGGATCCTCCCAAAGTGCTGGGATTACAGGT3′ and 5′GCGCGTCGACAACATGCTCTTGGCTCTGCCTTTG3′) and WI-26 genomic DNA template, and cloned into pGINT after *BamH*I and *Sal*I restriction enzyme digestion. The constructed plasmid pGINT-exon 2 which contains wild type AIMP2 exon 2 with the flanking intron regions was used as a template for site-directed mutagenesis to introduce each of the mutations identified from the WI-26T cells. To assess the effect of mutations on the generation of AIMP2-DX2, 0.5 μg of pGINT-EX2 wild type and its mutant derivatives were transfected into HEK293 cells seeded on a 6-well plate using GenePORTER reagent (Gelantis). The same amount of pRINT was transfected as a splicing and transfection control. After 24 hours incubation, the cells were visualized under fluorescent microscope to detect green and red fluorescence. The same set of transfected cells were used for RNA extraction using RNA extraction kit (Qiagen) and cDNA synthesis. Primer pairs, 5′ACGTAAACGGCCACAAGTTC3′ and 5′AAGTCGTGCTGCTTCATGTG 3′, were used for the detection of EGFP or exon 2-included EGFP transcripts.

Sequence analysis for exonic splicing enhancer (ESE) motifs

Wild type sequence of AIMP2 exon 2 from WI-26 and the exon 2 sequence with mutations found from WI-26T were analyzed for exonic splicing enhancer (ESE) of four serine/arginine-rich (SR) proteins. ESE finder program ver. 3.0 was used for the prediction. The highest sequence score for each SR protein was calculated in a random-sequence pool and the threshold values were set as the median of the highest score. The threshold values were as follows: SF2/ASF heptamer motif, 1.956; SF2/ASF (IgM-BRCA1) heptamer motif, 1.867; SC35 octamer motif, 2.383; SRp40 heptamer motif, 2.670; and SRp55 hexamer motif, 2.676.

RNA immunoprecipitation assay

HEK293T cells were transfected with GFP-tagged SF/ASF as well as pGINT-exon 2 or pGINT-exon 2 with A152G mutation (pGINT-A152G). After 24 h incubation, nuclear fraction was obtained and subjected to immunoprecipitation using anti-GFP antibody. GFP-SF2/ASF-bound mRNAs were purified using Trizol reagent according to the manufacturer's guideline. Reverse transcriptase PCR was conducted using AIMP2 exon 2-specific primers. To verify the effect of A152G mutation on the interaction with SF2/ASF *in vitro*, RNA probes encompassing full sequence of AIMP2 exon 2 were synthesized by *in vitro* transcription using [α-^{32}P]UTP and T7 promoter-containing DNA templates obtained from PCR amplification of pGINT-exon 2 WT and A152G. The RNA probes were incubated at 30°C for 30 min with GFP-SF2/ASF which was immunoprecipitated as mentioned above. After washing 3 times with the reaction buffer (20 mM HEPES, pH 7.8, 200 mM KCl, 20 mM NaCl, 10% glycerol, 2 mM DTT, and 2 mM $MgCl_2$) containing 0.05% NP-40, the RNA-protein complex was eluted using formaldehyde sample buffer, separated by electrophoresis in 7.5% urea polyacrylamide gel, and detected by autoradiography.

Generation of transgenic mice constitutively expressing AIMP2-DX2

Murine AIMP2/p38 sequence (BC026972) lacking exon 2 was cloned into pCDNA3.1(+) (Invitrogen) at *Hin*dIII and *Xho*I. The region of CMV promoter to poly A site was linearized and injected into mouse fertilized egg of C57BL/6 strain. The insertion of AIMP2-DX2 was confirmed by Southern blot and PCR analyses using the genomic DNA isolated from MEF cells. AIMP2-DX2 expression was determined by Northern and Western blot analyses (see Figure S3 for details).

Non-invasive imaging of cancer growth using bioluminescence

A549 cells expressing luciferase reporter (10^7) were injected into tail veins of five-week-old female BALB/c nu/nu mice. After 5–6 weeks, the dissemination of the cells was monitored by IVIS (Xenogen). Mice were divided into two group (n = 5/group) depending on their releasing photon flux and the mixtures of si-scramble AIMP2-DX2 (50 μg) or si-AIMP2-DX2 (50 μg) with GDM-PEI (glycerol dimethacrylate polyethyleneimine) [39] in 50 μl of 0.9% saline were delivered intratracheally into lung. To monitor photon flux, mice were anesthetized with isoflurane inhalation, and 100 ul of D-luciferin (7.5 mg/ml, Xenogen) were intraperitoneally (i.p.) injected. Bioluminescence imaging with

CCD camera (IVIS, Xenogen) was initiated 30 min after injection for 1–60 seconds, depending on the amount of luciferase activity. The data were expressed as photon-flux (photons/s/cm2/steradian).

Intratumoral injection of siRNA

For xenograft experiment, NCI-H460 lung cancer cells (10^7) were suspended in 200 µl of 0.9% saline and subcutaneously injected into 6 weeks old female nude mice. The tumor volumes were monitored three times a week. 50 µg of siRNA mixed with GDM-PEI were directly injected into tumors in three directions for four times in the indicated interval from the point that tumor volume reached 250 mm^3. The volume was calculated by (length x width x height)/2.

Gene delivery by intranasal inhalation

We designed shRNA against AIMP2-DX2 (TCGAGCGGGCCACGTGCAGGACTA TTCAAGAGATAGTCCTGCACGTGGCCCGCTTTT, underlined regions are matched to the DX2 sequence) and cloned into IMT-700 vector system (Imgenex) using *Sal*I and *Xba*I. The plasmid was mixed with glucosylated polyethyleneimine (G-PEI) at 1.64:1 weight ratio. After 1 week from last chemical injection, the DNA mixture was delivered into lung through intranasal pathway using the humid vacuum chamber in which the DNA mixture was vaporized. The DNA vapor was inhaled for 30 minutes through the nose of the mice that were fixed in the cylinder using Bio-Rad compressor as previously described [40]. From 6 weeks after the last injection of BP, the administration of DNA was conducted twice a week for 4 weeks and the tumor areas were measured.

Analysis of AIMP2-DX2 expression in lung cancer patients

To determine expression ratios of AIMP2-DX2 to AIMP2-F in different lung cancer stages, cDNAs from the frozen tissues of 23 patients with squamous cell carcinoma and adenocarcinoma were provided from Roswell Cancer Park Institute and analyzed by real-time PCR as described above. The research subject was reviewed and determined to be non-human subject research (NHSR) by the committee for Research Subject Protection of the Institute. Correlation of AIMP2-DX2 expression with patient survival was also investigated. This study included patients (n = 97) with pathological stages I, II or IIIA NSCLC patients who underwent curative surgical resection at the Kyungpook National University Hospital (Daegu, Korea) between January 2001 and December 2008. Patients who underwent chemotherapy or radiotherapy prior to surgery were excluded to avoid the effects on DNA. All the tissues were obtained at the time of surgery and then rapidly frozen in liquid nitrogen and stored at -80°C until the relevant bioassays were conducted. The histologic types of lung cancers, according to the World Health Organization classifications, were as follows: 44 cases (45.4%) of squamous cell carcinomas and 53 cases (54.6%) of adenocarcinomas. The pathologic staging of the tumors, which was determined according to the standard of the American Joint Committee on Cancer (AJCC), was as follows: 59 patients (60.8%) of stage I, 20 patients (21.6%) of stage II and 18 patients (18.6%) of stage IIIA. Written informed consent was obtained from all patients prior to surgery and this study was approved by the Institutional Review Board of the Kyungpook National University Hospital. Overall survival (OS) was measured from the day of surgery until the date of death or to the date of the last follow-up. Disease-free survival (DFS) was calculated from the day of surgery until recurrence or death from any cause. The survival estimates were calculated using the Kaplan-Meier method. The differences in OS or DFS across different genotypes were compared using the log-rank test. Hazard ratios (HRs) and 95% confidence intervals (CIs) were estimated using multivariate Cox proportional hazards models, with adjustment for age (≤63 versus >63 years), gender (male versus female), smoking status (never- versus ever-smoker), and pathologic stage (I versus II-IIIA). All analyses were performed using Statistical Analysis System for Windows, version 9.1 (SAS Institute, Cary, NC, USA).

Ethics statement

All human subject researches were approved by the appropriate ethics committees according to the Declaration of Helsinki. The correlation of AIMP2-DX2 expression with patient survival rate was studied under the review of institutional board in Kyungpook National University Hospital. The title was 'Identification of Cancer Specific Biomarker in Lung Cancer: 74005-263'. Roswell Park Cancer Institute approved the project 'Evaluation of AIMP2-DX2 as a Cellular marker for Diagnosis of Lung Cancer: NHR002008′ through their ethics committee.

Supporting Information

Figure S1 Sequences of AIMP2 exons and PCR primers. The primer DX2-S2 contains 14 bases of the 3′ end of exon 1 and 6 bases of the 5′ end of exon 3. The primer binding sites are indicated in red letters.
Found at: doi:10.1371/journal.pgen.1001351.s001 (0.12 MB TIF)

Figure S2 The mutations induced by BPDE treatment of WI-26 cells and their locations in exon 2 and intron 2 of AIMP2 gene. The first base of exon 2 was counted as position 1.
Found at: doi:10.1371/journal.pgen.1001351.s002 (0.02 MB TIF)

Figure S3 *Trans*-acting splicing factor, SF2/ASF, and *cis*-acting exon 2 mutations are involved in exon 2 skipping. (A) High score SR protein motifs in AIMP2 exon 2. The sequences of AIMP2 exon 2 in WI-26 as well as those with mutations found in WI-26T were analyzed to detect the ESE of four SR proteins using ESE Finder program ver. 3.0. Motif scores reflect the extent of matching to a degenerate consensus, and only the scores above the threshold for each SR protein are shown. Locations of point mutation found in WI-26T are indicated by asterisks. Deletion of C39 which is located in the ESE site of SF2/ASF (pink, left panel) increased the possibility of new ESE sites of SF2/ASF (red, right panel), SC35 (blue, right panel) and SRp40 (green, right panel) instead of losing original SF2/ASF site. A152G mutation, however, made all the ESE scores of its own sequence below threshold, as shown in SF2/ASF (red and pink, left panel) and SRp55 (yellow, left panel) sites. ESE of SF2/ASF is mostly affected by the A152G mutation in that three bars for ESE of SF2/ASF are disappeared (right panel). The width of each bar, length of the motif; the placement of each bar along the x axis, the position of a motif along the exon DNA sequence; and the height of the bar, the numerical score in the y axis. (B and C) Effects of SF2/ASF on the cellular levels of AIMP2-F and -DX2. (B) SF2/ASF was knocked down in H460 cells using specific si-RNA and the two protein levels were monitored by immunoblotting. (C) GFP-SF2/ASF was transfected in H460 cells and its effect on the levels of AIMP2-F and -DX2 was monitored as above. (D and E) A152G mutation in AIMP2 exon 2 reduced binding affinity of AIMP2 exon 2 to SF2/ASF. (D) mRNAs bound to immunoprecipitated GFP-SF2/ASF were purified and detected by RT-PCR using exon 2-specific primers. Exon 2 sequences were only amplified only in the samples from HEK 293T cells transfected with both GFP-SF2/ASF and pGINT-exon 2. No band was detected from the cells where GFP-

SF2/ASF and pGINT-A152G were expressed together. (E) Full-length AIMP2 exon 2 sequences with or without A152G mutation were radioactively synthesized as RNA probes and incubated with immunoprecipitated GFP-SF2/ASF *in vitro*. WT probe associated with SF2/ASF emanating strong signal while RNA probe with A152G mutation did not.
Found at: doi:10.1371/journal.pgen.1001351.s003 (0.56 MB TIF)

Figure S4 Etoposide-induced cell death is increased by knock-down of AIMP2-DX2 in p53-dependent manner. (A) After transfection with si-AIMP2-DX2, same number of cells was seeded and treated with etoposide. Cell viability was measured by MTT assay. (B) After transfection with si-AIMP2-DX2 in HCT116 p53+/- or p53-/- cells, same number of cells was seeded and treated with etoposide. Cell viability was measured by MTT assay.
Found at: doi:10.1371/journal.pgen.1001351.s004 (0.14 MB TIF)

Figure S5 Genomic incorporation of AIMP2-DX2-encoding cDNA was confirmed by Southern blotting (upper panel). Genomic DNA from AIMP2-DX2 transgenic mice was digested by *Hin*d III, and the resulting DNA fragments were separated by agarose gel electrophoresis and then transferred to hi-bond membrane (Amersham). After baking for 2 hours at 80°C, the membrane was processed as described in Brightstar Biodetect nonisotopic detection kit (Ambion). Probe conjugated with biotin was synthesized as suggested in BrightStar Psoralen-biotin nonisotopic labeling kit. Briefly, probe was produced by PCR using primer 5′AGGTAAAGCCCTATCATGGAGGCA3′ and 5′ACAGAGAGAACAG GAAACGTGCGA3′ specific to mouse AIMP2 gene (BC026972). For additional confirmation, we performed PCR by primer sequences on CMV vector promoter and AIMP2-DX2 structural gene. The sequences of forward and reverse primers are 5′ CGC TAT TAC CAT GGT GAT GCG 3′ and 5′ CGA ATG TGT GTG CAC AGT GGA 3′, respectively (middle panel). The expression of AIMP2-F and –DX2 were also determined by Western blot analysis (lower panel).
Found at: doi:10.1371/journal.pgen.1001351.s005 (0.12 MB TIF)

Figure S6 The effect of si-DX2 on the expression level of AIMP2-F and –DX2. The expression levels of AIMP2-F and –DX2 were quantified by quantitative realtime PCR as described in Materials and Methods.
Found at: doi:10.1371/journal.pgen.1001351.s006 (0.03 MB TIF)

Figure S7 The effect of sh-DX2 on the expression level of AIMP2-F and –DX2. The mRNAs were prepared from paraffin embedded lung tissues and the transcript levels of AIMP2-F and –DX2 were determined by semi-quantitative RT-PCR and gel electrophoresis.
Found at: doi:10.1371/journal.pgen.1001351.s007 (0.06 MB TIF)

Figure S8 Delivery of GFP-expressing plasmid to the various parts of mouse lung via intranasal inhalation. (A) GFP-encoding plasmid was delivered into mouse lung via intranasal inhalation as described. After 2 days, the mice were sacrificed and various regions of the lungs were fixed by paraffin block. The plasmid delivery was then monitored by fluorescence. About 50% of the examined lung area was evaluated as GFP positive. (B) The GFP-encoding plasmid delivery was also confirmed by green fluorescence in alveoli structure. (C) The delivery of the sh-DX2 encoding plasmid DNA was also confirmed by PCR. The lungs were isolated after intranasal delivery of the plasmid and the presence of the plasmid was confirmed by PCR. Left lane indicates the PCR product of the purified sh-AIMP2-DX2 encoding plasmid with the specific primers. Middle and right lanes indicate the PCR product of the DNAs isolated from the lungs isolated from the mice that received sh-AIMP2-DX2 plasmid and EV via intranasal inhalation, respectively. The PCR product with the primers specific to the AIMP2 promoter sequence of the endogenous genomic DNA was used as the control for PCR.
Found at: doi:10.1371/journal.pgen.1001351.s008 (1.37 MB TIF)

Figure S9 AIMP2-DX2 suppressed the effects of AIMP-F on p53 and FBP/c-myc. (A) A549 cells were transfected with myc-tagged AIMP2-F and -DX2. Cells were lysed and subjected to SDS-PAGE, followed by immunoblotting with anti-p53, anti-FBP, and anti-c-Myc antibodies. (B) A549 cells were transfected with myc-tagged AIMP2-F, -DX2 and HA-Ub. P53 was immnoprecipitated with anti-p53 antibody (FL-393) and then immunoprecipitates were subjected to SDS-PAGE and immunoblotting with anti-HA antibody. (C) A549 cells were transfected with myc-tagged AIMP2-F, -DX2 and HA-Ub. FBP was immnoprecipitated with anti-FBP and then immunoprecipitates were subjected to SDS-PAGE and immunoblotting with anti-HA antibody. (D) Cells (WI-26, H460, H1975 and H292) were lysed and the proteins were separated by SDS-PAGE, followed by immunoblotting with anti-AIMP2-F, -DX2, anti-p53, anti-SF2/ASF, and anti-c-Myc antibodies.
Found at: doi:10.1371/journal.pgen.1001351.s009 (1.14 MB TIF)

Table S1 Multivariate analysis for overall survival and disease free survival by demographics, smoking status, histological type, and pathologic stage.
Found at: doi:10.1371/journal.pgen.1001351.s010 (0.05 MB TIF)

Author Contributions

Conceived and designed the experiments: JWC JMH SK. Performed the experiments: JWC DGK AEL HRK JYL NHK YKS SHO BK HSJ BJP. Analyzed the data: JWC NHK YKS YLC SYK JYP JMH SK. Contributed reagents/materials/analysis tools: SKH SHC MHC JK HPK. Wrote the paper: JWC JMH SK.

References

1. Stetefeld J, Ruegg MA (2005) Structural and functional diversity generated by alternative mRNA splicing. Trends Biochem Sci 30: 515–521.
2. Nissim-Rafinia M, Kerem B (2005) The splicing machinery is a genetic modifier of disease severity. Trends Genet 21: 480–483.
3. Schwerk C, Schulze-Osthoff K (2005) Regulation of apoptosis by alternative pre-mRNA splicing. Mol Cell 19: 1–13.
4. Park SG, Ewalt KL, Kim S (2005) Functional expansion of aminoacyl-tRNA synthetases and their interacting factors: new perspectives on housekeepers. Trends Biochem Sci 30: 569–574.
5. Lee SW, Cho BH, Park SG, Kim S (2004) Aminoacyl-tRNA synthetase complexes: beyond translation. J Cell Sci 117: 3725–3734.
6. Han JM, Lee MJ, Park SG, Lee SH, Razin E, et al. (2006) Hierarchical Network between the Components of the Multi-tRNA Synthetase Complex: IMPLICATIONS FOR COMPLEX FORMATION. J Biol Chem 281: 38663–38667.
7. Park SG, Kang YS, Ahn YH, Lee SH, Kim KR, et al. (2002) Dose-dependent biphasic activity of tRNA synthetase-associating factor, p43, in angiogenesis. J Biol Chem 277: 45243–45248.
8. Ko Y-G, Park H, Kim T, Lee J-W, Park SG, et al. (2001) A cofactor of tRNA synthetase, p43, is secreted to up-regulate proinflammatory genes. J Biol Chem 276: 23028–32303.
9. Park H, Park SG, Lee J-W, Kim T, Kim G, Ko Y-G, Kim S (2002) Monocyte Cell Adhesion Induced by a Human Aminoacyl-tRNA Synthetase Associated Factor, p43: Identification of the Related Adhesion Molecules and Signal Pathways. J Leukoc Biol 71: 223–230.
10. Park SG, Shin H, Shin YK, Lee Y, Choi EC, et al. (2005) The Novel Cytokine p43 Stimulates Dermal Fibroblast Proliferation and Wound Repair. Am J Pathol 166: 387–398.
11. Park SG, Kang YS, Kim JY, Lee CS, Ko YG, et al. (2006) Hormonal activity of AIMP1/p43 for glucose homeostasis. Proc Natl Acad Sci U S A 103: 14913–14918.
12. Han JM, Park SG, Liu B, Park BJ, Kim JY, et al. (2007) Aminoacyl-tRNA Synthetase-Interacting Multifunctional Protein 1/p43 Controls Endoplasmic Reticulum Retention of Heat Shock Protein gp96: Its Pathological Implications in Lupus-Like Autoimmune Diseases. Am J Pathol 170: 2042–2054.

13. Park BJ, Kang JW, Lee SW, Choi SJ, Shin YK, et al. (2005) The haploinsufficient tumor suppressor p18 upregulates p53 via interactions with ATM/ATR. Cell 120: 209–221.
14. Kim KJ, Park MC, Choi SJ, Oh YS, Choi EC, et al. (2008) Determination of three dimensional structure and residues of novel tumor suppressor, AIMP3/p18, required for the interaction with ATM. J Biol Chem.
15. Park BJ, Oh YS, Park SY, Choi SJ, Rudolph C, et al. (2006) AIMP3 haploinsufficiency disrupts oncogene-induced p53 activation and genomic stability. Cancer Res 66: 6913–6918.
16. Kim MJ, Park B-J, Kang Y-S, Kim HJ, Park J.-H, Kang JW, Lee SW, Han JM, Lee H-W, Kim S (2003) Downregulation of fuse-binding protein and c-myc by tRNA synthetase cofactor, p38, is required for lung differentiation. Nature Genetics 34: 330–336.
17. Han JM, Park BJ, Park SG, Oh YS, Choi SJ, et al. (2008) AIMP2/p38, the scaffold for the multi-tRNA synthetase complex, responds to genotoxic stresses via p53. Proc Natl Acad Sci U S A 105: 11206–11211.
18. Choi JW, Kim DG, Park MC, Um JY, Han JM, et al. (2009) AIMP2/p38 promotes TNF-alpha-dependent apoptosis via ubiquitin-mediated degradation of TRAF2. J Cell Sci 122: 2710–2715.
19. Choi JW, Um JY, Kundu JK, Surh YJ, Kim S (2009) Multidirectional tumor-suppressive activity of AIMP2/p38 and the enhanced susceptibility of AIMP2 heterozygous mice to carcinogenesis. Carcinogenesis 30: 1638–1644.
20. Kwon MJ, Oh E, Lee S, Roh MR, Kim SE, et al. (2009) Identification of novel reference genes using multiplatform expression data and their validation for quantitative gene expression analysis. PLoS ONE 4: e6162. doi:10.1371/journal.pone.0006162.
21. Bonano VI, Oltean S, Garcia-Blanco MA (2007) A protocol for imaging alternative splicing regulation in vivo using fluorescence reporters in transgenic mice. Nat Protoc 2: 2166–2181.
22. Cartegni L, Wang J, Zhu Z, Zhang MQ, Krainer AR (2003) ESEfinder: A web resource to identify exonic splicing enhancers. Nucleic Acids Res 31: 3568–3571.
23. Smith PJ, Zhang C, Wang J, Chew SL, Zhang MQ, et al. (2006) An increased specificity score matrix for the prediction of SF2/ASF-specific exonic splicing enhancers. Hum Mol Genet 15: 2490–2508.
24. Karni R, de Stanchina E, Lowe SW, Sinha R, Mu D, et al. (2007) The gene encoding the splicing factor SF2/ASF is a proto-oncogene. Nat Struct Mol Biol 14: 185–193.
25. Karni R, Hippo Y, Lowe SW, Krainer AR (2008) The splicing-factor oncoprotein SF2/ASF activates mTORC1. Proc Natl Acad Sci U S A 105: 15323–15327.
26. Pio R, Montuenga LM (2009) Alternative splicing in lung cancer. J Thorac Oncol 4: 674–678.
27. Quevillon S, Robinson J-C, Berthonneau E, Siatecka M, Mirande M (1999) Macromolecular assemblage of aminoacyl-tRNA synthetases: Identification of protein-protein interactions and characterization of a core protein. J Mol Biol 285: 183–195.
28. Park SG, Jung KH, Lee JS, Jo YJ, Motegi H, et al. (1999) Precursor of pro-apoptotic cytokine modulates aminoacylation activity of tRNA synthetase. J Biol Chem 274: 16673–16676.
29. Li HR, Wang-Rodriguez J, Nair TM, Yeakley JM, Kwon YS, et al. (2006) Two-dimensional transcriptome profiling: identification of messenger RNA isoform signatures in prostate cancer from archived paraffin-embedded cancer specimens. Cancer Res 66: 4079–4088.
30. Nanjundan M, Zhang F, Schmandt R, Smith-McCune K, Mills GB (2007) Identification of a novel splice variant of AML1b in ovarian cancer patients conferring loss of wild-type tumor suppressive functions. Oncogene 26: 2574–2584.
31. Tacconelli A, Farina AR, Cappabianca L, Desantis G, Tessitore A, et al. (2004) TrkA alternative splicing: a regulated tumor-promoting switch in human neuroblastoma. Cancer Cell 6: 347–360.
32. Ghosh A, Stewart D, Matlashewski G (2004) Regulation of human p53 activity and cell localization by alternative splicing. Mol Cell Biol 24: 7987–7997.
33. Bourdon JC, Fernandes K, Murray-Zmijewski F, Liu G, Diot A, et al. (2005) p53 isoforms can regulate p53 transcriptional activity. Genes Dev 19: 2122–2137.
34. Park BJ, Lee SJ, Kim JI, Lee CH, Chang SG, et al. (2000) Frequent alteration of p63 expression in human primary bladder carcinomas. Cancer Res 60: 3370–3374.
35. Yang A, Schweitzer R, Sun D, Kaghad M, Walker N, et al. (1999) p63 is essential for regenerative proliferation in limb, craniofacial and epithelial development. Nature 398: 714–718.
36. Mills AA, Zheng B, Wang XJ, Vogel H, Roop DR, et al. (1999) p63 is a p53 homologue required for limb and epidermal morphogenesis. Nature 398: 708–713.
37. Park SG, Schimmel P, Kim S (2008) Aminoacyl tRNA synthetases and their connections to disease. Proc Natl Acad Sci U S A 105: 11043–11049.
38. Park SG, Choi EC, Kim S (2010) Aminoacyl-tRNA synthetase-interacting multifunctional proteins (AIMPs): a triad for cellular homeostasis. IUBMB Life 62: 296–302.
39. Arote RB, Hwang SK, Yoo MK, Jere D, Jiang HL, et al. (2008) Biodegradable poly(ester amine) based on glycerol dimethacrylate and polyethylenimine as a gene carrier. J Gene Med 10: 1223–1235.
40. Kim HW, Park IK, Cho CS, Lee KH, Beck GR, Jr., et al. (2004) Aerosol delivery of glucosylated polyethylenimine/phosphatase and tensin homologue deleted on chromosome 10 complex suppresses Akt downstream pathways in the lung of K-ras null mice. Cancer Res 64: 7971–7976.
41. Kwon TK, Nordin AA (1998) Identification of cdk2 binding sites on the p27Kip1 cyclin-dependent kinase inhibitor. Oncogene 16: 755–762.